Catalysis Letters, Vol. 115, Nos. 1–2, May 2007 (© 2007)
DOI: 10.1007/s10562-007-9075-z

Autothermal reforming of *n*-dodecane, toluene, and their mixture on mono- and bimetallic noble metal zirconia catalysts

Reetta K. Kaila, A. Gutiérrez, S. T. Korhonen, and A. O. I. Krause

Laboratory of Industrial Chemistry, Helsinki University of Technology (TTK), P.O. Box 6100, Helsinki 02015, Finland

Received 2 March 2007; accepted 2 March 2007

Autothermal reforming (ATR) of higher hydrocarbons and their mixture was studied on zirconia-supported mono- (Rh, Pd, or Pt) and bimetallic (RhPt) catalysts. ATR reactions predominated on Rh-containing catalysts at 700–900 °C, whereas thermal cracking predominated on Pt and the support. The thermal stability of Rh was improved when Rh was combined with Pt in the bimetallic catalyst.

KEY WORDS: autothermal reforming; *n*-dodecane; toluene; hydrocarbon mixture; zirconia; bimetallic; noble metal catalysts; DRIFTS; chemisorption; FT-IR.

1. Introduction

Energy demand continues to climb as the world population grows. Meanwhile, oil reserves are diminishing. Developing new energy sources and more efficient technologies is thus of paramount importance. At the same time, the level of emissions and exhaust gases needs to be reduced to minimize their contribution to the greenhouse effect. Environmentally friendly energy solutions are being sought, especially for mobile applications. Indeed, internal combustion engines could be replaced with more efficient fuel cell engines such as high temperature solid oxide fuel cells (SOFCs) e.g. in ships, or fuel cells could be used as auxiliary power units (APUs). The combination of an on-board reformer and a SOFC would enable commercial fuels such as diesel to be used as a hydrogen source. Easy to deliver and safe to store, and with an infrastructure already in place, commercial fuels could be a good first step toward a hydrogen-based society [1–3].

Steam reforming (SR) of "high molecular weight hydrocarbons" (light distillate naphtha) has been practiced for over 40 years in locations where natural gas is not available [4]. However, autothermal reforming (ATR) of higher hydrocarbons is preferable to SR since it combines highly endothermic SR (equation 1) with exothermic partial oxidation (POX; equation 2) [3,5,6]. This means that ATR is thermally more stable than SR and can be driven to thermoneutral conditions. In addition, the start-up of ATR is rapid [3].

$$C_xH_y + xH_2O \Leftrightarrow \left(x + \frac{1}{2}y\right)H_2 + xCO \qquad (1)$$

$$C_xH_y + \frac{1}{2}xO_2 \Leftrightarrow \frac{1}{2}yH_2 + xCO \qquad (2)$$

Noble metals, especially Rh catalysts, are active in the reforming of hydrocarbons to synthesis gas [3,7–9]. And unlike conventional nickel catalysts, they tolerate sulfur [3,10] and prevent coke deposition [3,7,11], these being necessary properties for any reforming catalyst used with a commercial fuel as feed. Commercial fuels contain sulfur that cannot be completely removed, as the sulfur is present in the aromatic ring [12]. Furthermore, on certain catalysts sulfur deposition tends to induce coke accumulation [12]. A significant drawback of noble metals is their cost. The price of rhodium has risen almost 10-fold over the past 3 years (from US$ 16.77 to 149.71 per gram annual average) [13].

The aim of our work was to study the ATR of higher hydrocarbons and their mixtures as a means of obtaining hydrogen-rich fuel gas (H_2, CO, CO_2, CH_4, and H_2O) suitable for solid oxide fuel cells (SOFCs) applications [7,14]. *n*-dodecane and toluene were used as model compounds for the aliphatic and aromatic fractions of commercial fuels. Zirconia-supported mono- (Rh, Pd, and Pt) and bimetallic (Rh and Pt) catalysts with low Rh loading were examined with the objective of finding a stable, active, and selective catalyst that also is economically viable.

2. Experimental

2.1. Catalyst preparation

The noble metal catalysts (Rh, Pd, Pt) were prepared by dry impregnation from 10 wt% $Rh(NO_3)_3$ solution

*To whom correspondence should be addressed.
E-mail: reetta.kaila@tkk.fi

diluted in 5 wt% nitric acid (Sigma-Aldrich), and from $Pd(NO_3)_2$ (Alfa-Aesar 8.5 wt%) and $Pt(NO_3)_4$ (Johnson-Matthey 16 wt%) solutions to obtain not more than 0.5% noble metal by weight. The ZrO_2 support (MEL Chemicals EC0100) was ground to particle size 0.250–0.355 mm and calcined at 900 °C for 16 h. The BET surface area of the support was 21.5 m^2/g and the total pore volume was 0.16 cm^3/g (physisorption, Coulter Omnisorp 100 CX). After impregnation, the catalysts were dried at room temperature for 4 h and at 100 °C overnight, and then calcined at 700 °C or 900 °C for 1 h (heating rate 80 °C/h). For comparison, platinum catalysts were also prepared from $Pt(NH_4)_4(NO_3)_2$ (Strem Chemicals 99 wt%) and $H_2(PtCl_6)$ (Merck (p.a) 3.8 wt%) precursors.

Two bimetallic RhPt catalysts, with total metal loading of not more than 0.5 wt%, were prepared by co-impregnation from $Rh(NO_3)_3$ and $Pt(NH_4)_4(NO_3)_2$ precursors. The Rh to Pt molar ratios of the bimetallic catalysts were 1.2 and 2.4 mol/mol. The performance of these bimetallic catalysts in ATR of the *n*-dodecane–toluene mixture was compared with the performance of Rh, Pd, and Pt catalysts and the ZrO_2 support.

2.2. Catalyst characterization

The noble metal loading of the catalysts was determined by inductively coupled plasma-atomic emission spectroscopy (ICP-AES). However, the low metal loading (< 0.5 wt%) of the catalysts affected the accuracy of the catalyst characterization.

2.2.1. Chemisorption

The H_2 (AGA 99.999%) and CO (Messer Griesheim 99.997%) chemisorption uptakes were measured with a Coulter Omnisorp 100 CX instrument. The chemisorption was performed at 30 °C in order to minimize the spillover of H_2 onto the support [15]. This was valid except for the palladium catalyst, where the H_2 chemisorption was performed at 100 °C to prevent the formation of palladium hydrides [16]. Before the recording of total chemisorption isotherms (15 steps between 0.6 kPa and 46.6 kPa), catalyst samples (0.2 g) were reduced in hydrogen and evacuated at 350 °C, in both cases for 2 h. A second isotherm indicating reversible chemisorption was measured after samples had been evacuated at 30 °C for 0.5 h. Both isotherms were extrapolated to zero pressure, and their difference was used as a measure of strongly chemisorbed H_2 or CO uptakes (irreversible). The metal dispersion was calculated with equation 3 by assuming 2:1 and 1:1 stoichiometry between the metal surface atom and the adsorbed H_2 and CO, respectively [17–20].

$$D = \frac{V_X St M_M}{V_m wt\%} 100\%, \quad (3)$$

where V_X is the irreversible uptake of H_2 or CO [ml/g_{cat}], V_m is 22.41 l/mol, St is the stoichiometric ratio (M:X) [mol/mol], M_M is the molar mass of the noble metal [g/mol], and wt% is the metal loading of the catalyst [g/g_{cat}].

2.2.2. In situ diffuse reflectance Fourier transform infrared spectroscopy

Carbon monoxide (Messer Griesheim 99.997%) adsorption was studied by *in situ* diffuse reflectance Fourier transform infrared spectroscopy (DRIFTS). The equipment consisted of a Nicolet Nexus Fourier transform infrared spectrometer equipped with a Spectra Tech reaction chamber with ZnSe windows for high temperatures and pressures. The DRIFT spectra were recorded from 400 cm^{-1} to 4000 cm^{-1} using a ground sample to enhance the quality of the spectra. The product gas stream was analyzed online with a Pfeiffer Vacuums OmniStar mass spectrometer (MS) scanning masses from 0 to 60. The experimental setup is described in more detail elsewhere [21]. The catalyst samples were calcined and reduced in situ in the reaction chamber with diluted air (10% O_2/N_2, synthetic air AGA 99.99% and nitrogen AGA 99.999% purified with Oxisorb, Messer Griesheim) for 2 h at 300 °C and with 7.4% hydrogen (AGA 99.999%) in nitrogen for 0.5 h at 300 °C. The total flow rate of the reactant gases was kept constant during all experiments at 50 cm^3/min. After the prereduction the samples were cooled down to 30 °C under nitrogen flow.

The carbon monoxide adsorption experiments were performed as sequences of carbon monoxide feed and nitrogen flushes. Carbon monoxide (5% CO/N_2) at 30 °C was fed to the reaction chamber while the spectrum was recorded with 100 scans using a spectrum of an aluminum mirror as the background (4 cm^{-1}, 200 scans). A 5 min flush with nitrogen followed. During the flush, spectra were recorded every minute (4 cm^{-1}, 30 scans). The sample was then heated slowly (~6 °C/min) in carbon monoxide feed and a new spectrum was recorded at 50 °C followed by a new nitrogen flush for 5 min. The sequences were continued by recording spectra under carbon monoxide (4 cm^{-1}, 100 scans) and nitrogen (30 scans) at 75 and 100 °C. The same sequences were repeated while the samples were cooled down to 30 °C at a rate of ~6 °C/min to ensure that the results were reproducible.

2.3. Catalyst testing in ATR

Testing of the noble metal catalysts and the zirconia support in ATR reactions was performed in a tubular quartz reactor at atmospheric pressure with temperatures set to 700–900 °C and with 0.1–0.2 g of catalyst. The reactor temperature was increased in steps of 50 °C, and finally it was set back to the initial temperature

(700 °C) to investigate the catalyst deactivation during the ATR cycle. After the ATR cycle, the catalyst was regenerated with air, and the product was analyzed. The formation of carbon dioxide and water during the regeneration step indicated coke accumulation.

The feed consisted of *n*-dodecane (Sigma-Aldrich 99 + %), toluene (Riedel-de Haën ≥ 99.7%), or their mixture, plus water and air. The aromatic content (toluene) of the mixture was 20 wt%. The H_2O/C and O_2/C feed ratios were 2.3–3 mol/mol and 0.34 mol/mol, respectively. These ratios were selected on the basis of optimization of reaction conditions and thermodynamic calculations to provide a thermoneutral ATR of *n*-dodecane at 700 °C and to minimize coke deposition [6,9,22]. The hydrocarbons and water were vaporized and mixed with air before introduction to the reactor. The total flow rate of the reactants was 300 cm^3/min (NTP), and the feed was diluted with argon to a total flow rate of 900 cm^3/min (NTP). Thus, the gas hourly space velocity (GHSV) was 3.0–5.9 × 10^5 L/h.

2.4. Product analysis

The product flow was diluted with nitrogen (900 cm^3/min NTP) to allow reliable detection of the hydrocarbons. The diluted stream was analyzed with a Gasmet Fourier transform infrared spectrometer (FT-IR, Gasmet™) equipped with a Peltier-cooled MCT detector and multicomponent analysis software [23,24]. The temperature of all the lines and the sample cell was set to 230 °C to keep the higher hydrocarbons in gas phase. Analyzed compounds were CO, CO_2, H_2O, CH_4, C_2H_2, C_2–C_8 alkanes, C_2–C_5 alkenes, C_2–C_4 alcohols, cyclohexane, methylcyclohexane, benzene, toluene, and *n*-dodecane. All oxygen was assumed to be consumed, since the O_2/C feed ratio was less than the stoichiometric ratio of the POX. The amount of hydrogen formed was calculated from the mass balances on the basis of the measured dry gas flow rate. The product distribution was calculated with equation (4), where n_i is the molar amount of product *i*:

$$S_i = \frac{n_i}{\sum n_i} \tag{4}$$

3. Results and discussion

3.1. Catalyst characterization

Table 1 shows the metal loadings determined by ICP-AES for the fresh and tested catalysts. The total metal loadings of the fresh Pd and Pt and bimetallic RhPt catalysts were close to the targeted amount (0.5 wt%), whereas the metal loadings of the monometallic Rh catalysts were only 0.22–0.25 wt%.

3.1.1. In situ DRIFTS measurements

Adsorption of carbon monoxide on the Rh, Pd, and Pt catalysts and on the ZrO_2 support was investigated to verify the stoichiometry of the CO adsorption to be used in the dispersion calculations. Figure 1 presents the adsorption results under carbon monoxide flow at 30 and 100 °C. No significant difference was observed in the type of the adsorbed CO species at the two temperatures. The bands observed at 30 °C and their assignments to different species are presented in table 2. No formation of carbon dioxide on the samples was observed in the studied temperature range.

Only linear CO was observed on the Pt catalyst, while both linear and bridged adsorption states were detected on our Pd catalyst. Bridged CO is usually the predominant adsorption state on Pd catalyst [20]. However, the fraction of each adsorption state (linear, bridged, multibonded) varies with the support, and, for instance, more adsorbed CO exists in linear (Pd:CO = 1:1) state on Pd/ZrO_2 than on Pd/Al_2O_3 [20]. All three adsorption states were observed on the Rh catalyst at both temperatures but their relative abundance was temperature dependent. The amount of $(CO)_2$–Rh^+ species was

Table 1
Metal loadings of fresh and tested ZrO_2-supported noble metal catalysts calcined at 700 °C

Catalyst	Fresh catalyst			Tested catalyst
	Metal loading		Rh/Pt (mol/mol)	Metal loading (μmol/g_{cat})
	(wt%)	(μmol/g_{cat})		
$Rh_{0.16}Pt_{0.26}$	0.16 (Rh), 0.26 (Pt)	15.9 (Rh), 13.3 (Pt)	1.2	15.1 (Rh), 12.9 (Pt)
$Rh_{0.21}Pt_{0.16}$	0.21 (Rh), 0.16 (Pt)	19.9 (Rh), 8.3 (Pt)	2.4	25.0 (Rh), 8.6 (Pt)
Rh	0.22	21.8		15.1
Rh (900)*	0.24	23.8		n.a.
Pd	0.41	38.7		78.2
Pt_A	0.45	22.9		21.4
Pt_B	0.46	23.4		20.9
Pt_C	0.46	23.4		–

Abbreviations: A = nitrate, B = tetraamine nitrate, C = hexachloro acid precursor.
*The calcination temperature was 900 °C.

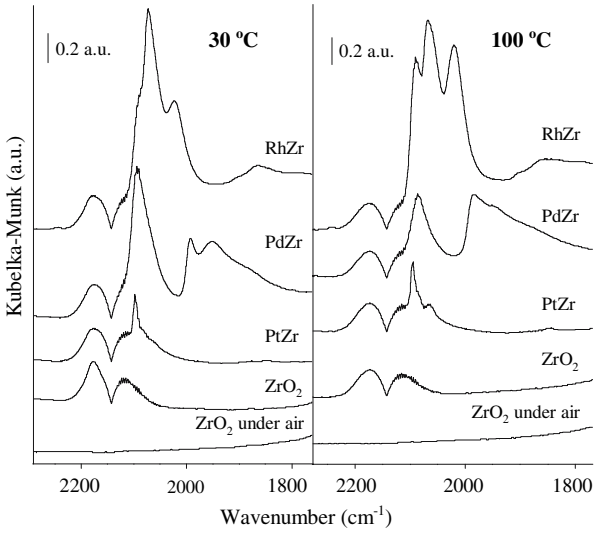

Figure 1. Carbon monoxide adsorption on H_2-reduced catalysts at 30 and 100 °C DRIFT spectra were recorded under CO.

observed to increase with increasing temperature as the band at 2090 cm^{-1} started to evolve (see figure 1, 100 °C) and the band at 2025 cm^{-1} increased in intensity.

On the basis of these results, the stoichiometric M:CO ratio for Rh and Pd cannot be assumed to be equal to 1:1. Some CO was observed to adsorb on the support. The amounts of the different adsorbed species could not be quantified from the DRIFT spectra.

3.1.2. Chemisorption

The H_2 and CO chemisorption uptakes of the monometallic catalysts are presented in table 3. High total uptakes of H_2 were obtained on all catalysts, which supports the earlier finding that H_2 adsorbs on redox supports like ZrO_2 in the presence of a metallic phase [29]. The adsorbed H_2 was bound very weakly, however, especially on the Pt catalysts and on the Rh catalyst calcined at 900 °C, since the difference between the total and reversible H_2 uptakes was small. H_2 must have been adsorbed on the support rather than the surface metal. Examination of the irreversible H_2 uptakes (table 3) shows nevertheless that the noble metal dispersions for 0.22 wt% Rh/ZrO_2 (28.3%) and 0.41% Pd/ZrO_2 (29.6%) calcined at 700 °C are of the same magnitude as those reported by Wei and Iglesia [30] for 0.2 wt% Rh/Al_2O_3 (43.4%) and 0.4 wt% Rh/Al_2O_3 (37.2%), and by Polychronopoulou *et al.* [31] for 0.5 wt% Rh/ZrO_2 (23%) catalysts. As the high calcination temperature (900 °C) had a degrading effect on the catalyst characteristics, the studies focused on catalysts calcined at 700 °C.

The CO chemisorption (table 3) was measured for comparison since the total CO adsorption at room temperature does not change the oxidation state of the

Table 2
Observed DRIFT bands in carbon monoxide adsorption experiments at 30 °C

	Observed adsorption at 30 °C				Adsorption at room temperature reported in literature			
	RhZr	PdZr	PtZr	ZrO_2	1.0 $RhZrO_2$ [25]	1.4 $PdAl_2O_3$ [26]	PtZrO2*	ZrO_2 [28]
CO-support	2181	2180	2180	2185	2192			2185
CO(L)-M	2073	2094	2098		2050	2072	2084 [27], 2068 [28]	
$(CO)_2$-M^+	2025				2090, 2020			
CO(B)-M	1865	1992, 1950			1890	1980, 1942		

Abbreviations: L = linear, B = bridged, M = metal. [25–28]
* Metal loading not reported.

Table 3
Hydrogen and carbon monoxide chemisorption uptakes on ZrO_2-supported noble metal catalysts calcined at 700 °C

Catalyst	H_2 uptake ($\mu mol/g_{cat}$)			CO uptake ($\mu mol/g_{cat}$)		
	Total	Reversible	Irreversible	Total	Reversible	Irreversible
Rh	122	119	3.1	146	120	25.7
Rh (900)*	111	110	0.5	–	–	–
Pd**	104	98	5.7	153	122	31.5
Pt_A	116	116	0.0	128	125	3.2
Pt_B	111	111	0.1	130	128	2.2
Pt_C	117	117	0.0	120	117	3.3
ZrO_2	109	107	1.5	125	121	4.6

Abbreviations: A = nitrate, B = tetraamine nitrate, C = hexachloro acid precursor.
* The calcination temperature was 900 °C.
** The H_2 chemisorption temperature was 100 °C.

support [29]. The results obtained for 0.22 wt% Rh/ZrO_2 (25.7 μmol/g_{cat}) and 0.41 wt% Pd/ZrO_2 (31.5 μmol/g_{cat}) are in good accordance with the CO uptakes of 26.8, 27.0, and 87.9 μmol/g_{cat} reported for 0.87 wt% Pt/$Ce_{0.6}Zr_{0.4}O_2$ [32], 1 wt% Pd/ZrO_2 [20], and 0.5 wt% Rh/TiO_2 [17], respectively. However, CO also adsorbed on the pure ZrO_2, and the irreversible uptake was of the same magnitude as measured for the Pt catalysts. According to Zhang *et al.* [17] CO adsorption on pure ZrO_2 is low. Moreover, the calculated dispersions (equation 3; Rh: 118.0%, Pd: 81.2%) were not comparable to those calculated from H_2 uptakes. According to the DRIFTS measurements, the bridged and multibonded adsorption states of CO were present on Rh [17,33]. The M:CO stoichiometric ratio could not be defined, therefore, and the metal dispersions could not be reliably calculated for our Rh catalysts.

3.2. ATR of n-dodecane, toluene, and their mixture on noble metal catalysts

3.2.1. Catalyst activity

In the ATR of single hydrocarbons and their mixture, complete conversions of *n*-dodecane and toluene were obtained on the Rh-containing catalysts even with the temperature set to 700 °C (table 4). However, the conversions remained lower, when the Rh catalyst was calcined at 900 °C (table 4). On all other catalysts complete conversion of *n*-dodecane with GHSV of 3.0×10^5 L/h was obtained only with reaction temperatures set to 800 °C or higher (figure 2a). In ATR of toluene, complete hydrocarbon conversion was obtained only on the Rh catalysts (figure 2b). In ATR of the hydrocarbon mixture (with 20 wt% of toluene), on the other hand, the conversion of toluene reached 100% on Rh at 700 °C, on Pd at 800 °C, and on Pt and ZrO_2 at 900 °C.

In thermoneutral ATR of single *n*-dodecane and toluene, the SR conversions at 700 °C are according to thermodynamics 28.6% and 46.6%, respectively; the rest of the feed reacts via POX [7]. Hence, the maximum conversion of water is 9.5% and 15.5%, respectively, when water is fed in 3-fold excess (H_2O/C = 3 mol/mol). In experiments on Rh-containing catalysts, however, higher conversions of water were obtained over the whole temperature range (figure 2) indicating high catalyst activity toward SR of both hydrocarbons. On the Rh catalyst calcined at 900 °C, the conversion of water

Table 4
Conversions and the main product distribution in ATR of the *n*-dodecane–toluene mixture with temperature set to 700 °C

Catalyst	$T_{catalyst\ bed}$ (° C)	Conversion (mol%)			Main product distribution (mol%)				
		$C_{12}H_{26}$	C_7H_8	H_2O	H_2	CO	CO_2	CH_4	C_2H_4
$Rh_{0.16}Pt_{0.26}$	720	100	100	29	59	15	26	0.3	0.0
$Rh_{0.21}Pt_{0.16}$	690	99	100	29	63	14	22	0.4	0.0
Rh	695	100	100	24	63	16	21	0.5	0.0
Rh (900)*	665	96	97	17	57	23	19	0.4	0.2
Pd	730	85	57	−3.1	54	30	12	1.1	1.8
Pt_A	760	78	28	−11	22	44	15	2.7	8.4
PtB	760	82	29	−10	17	46	17	2.9	9.5
ZrO_2	700	83	28	−3.7	16	39	12	4.3	14

GHSV = 3.0×10^5 L/h, H_2O/C = 2.3 mol/mol. Abbreviations: A = nitrate, B = tetraamine nitrate precursor.
* The calcination temperature was 900 °C.

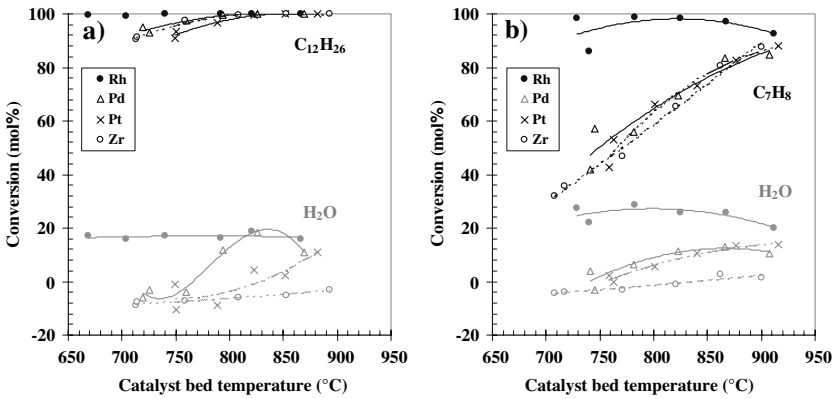

Fig. 2 Conversions of hydrocarbons (black) and water (gray) in ATR of (a) *n*-dodecane and (b) toluene on Rh (●), Pd (△), Pt_A (×), and ZrO_2 (○) catalysts. GHSV = 3.0×10^5 L/h, H_2O/C = 3 mol/mol.

remained lower (table 4), which reveals a decrease in the SR activity, in accordance with the chemisorption results. On Pd and Pt catalysts and the support, the conversion of water was negative at 700 °C (table 4) indicating that water was formed extensively and oxidation reactions were taking place. These oxidation reactions affected the total reaction enthalpy and the thermal stability of the ATR system. The conversion of water increased with temperature, however, on Pd reaching a maximum at 800–850 °C. The Pt catalyst behaved in a similar way to the pure support at temperatures below 800 °C (table 4), but it became active toward ATR at higher temperatures (table 5); water was formed on the support over the whole temperature range. At higher temperatures, the activities of the Pt and Pd catalysts were still lower than the activities of the Rh-containing catalysts (table 5).

The effect of catalyst precursor (A: $Pt(NO_3)_4$, B: $Pt(NH_4)_4(NO_3)_2$, and C: $H_2(PtCl_6)$) was studied in an attempt to improve the Pt catalyst performance. The metal precursor had no noticeable effect on the performance of the catalyst, as also reported by Guglielminotti *et al*. [34]. No difference in the H_2 and CO chemisorption uptakes of these three catalysts was noticed either (table 3). Thus, the catalyst calcination at 700 °C was effective and we assume that no residues of precursors remained on any catalyst.

3.2.2. Catalyst selectivity

The main products in the ATR of *n*-dodecane, toluene, or their mixture were H_2, CO, and CO_2. Additionally, minor amounts of thermal cracking products were formed when the ATR feed contained *n*-dodecane, and the catalyst activity was low.

The amounts of H_2 and C_2H_4 in the product revealed the existence of ATR reactions and thermal cracking, respectively. The concentrations of these products obtained in ATR of the hydrocarbon mixture are depicted in figure 3. The Rh-containing catalysts were most selective for H_2 production owing to their high SR activity; scarcely any cracking products were detected (tables 4 and 5). The highest concentration of H_2 was observed on the bimetallic $Rh_{0.21}Pt_{0.16}$ catalyst. With lower Rh loading ($Rh_{0.16}Pt_{0.26}$), the selectivities for the main products were lower over the whole temperature range, and thermal cracking products were detected at higher temperatures (table 5). In ATR of *n*-dodecane and the *n*-dodecane–toluene mixture, the formation of

Table 5
Conversions and the main product distribution in ATR of the *n*-dodecane–toluene mixture with temperature set to 900 °C

Catalyst	$T_{catalyst\ bed}$ (° C)	Conversion (mol%)			Main product distribution (mol%)				
		$C_{12}H_{26}$	C_7H_8	H_2O	H_2	CO	CO_2	CH_4	C_2H_4
$Rh_{0.16}Pt_{0.26}$	890	100	100	28	63	18	17	1.2	0.7
$Rh_{0.21}Pt_{0.16}$	880	100	100	28	65	17	18	0.4	0.0
Rh	875	100	100	30	64	16	20	0.7	0.0
Rh (900)*	860	100	100	26	51	25	23	0.8	0.0
Pd	880	100	100	23	57	30	12	0.6	0.0
Pt_A	885	100	100	14	53	35	7.0	3.1	1.1
Pt_B	880	100	100	15	55	35	7.2	2.1	0.7
ZrO_2	900	100	99	−0.9	38	36	4.2	9.8	10

GHSV = 3.0×10^5 L/h, H_2O/C = 2.3 mol/mol. Abbreviations: A = nitrate, B = tetraamine nitrate precursor.
* The calcination temperature was 900 °C.

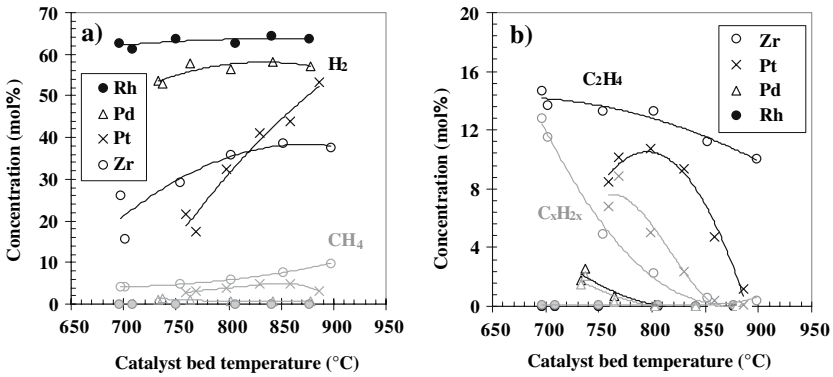

Fig. 3 ATR of the *n*-dodecane–toluene mixture, product concentrations of (a) hydrogen and methane and (b) ethene and other (C_3–C_5) alkenes (C_xH_{2x}) on Rh (●), Pd (△), Pt_A (×), and ZrO_2 (○) catalysts. GHSV = 3.0×10^5 L/h, H_2O/C = 2.3 mol/mol. Abbreviation: A = nitrate precursor.

methane, ethene, and other alkenes (C_3–C_5) on the catalysts increased in the order Rh < Pd < Pt < ZrO_2, indicating low catalytic activity of the support and the Pt catalysts toward ATR reactions (figure 3). These results are in agreement with the H_2 and CO uptakes, which were much lower on the Pt catalysts and the ZrO_2 support than on the Pd and Rh catalysts (table 3).

The concentrations of alkenes decreased and the concentrations of H_2 increased with temperature (figure 3), together with the improvement in catalyst activity. The increase in temperature seemed to affect the performance of the Pt catalyst in particular, since a plateau appeared on the concentration curves of the thermal cracking products (figure 3). No thermal cracking products were formed in ATR of toluene, moreover. However, some toluene cleaved to methane and benzene on the support, and with the GHSV of 5.9×10^5 L/h also on the Rh catalyst.

Even though almost complete hydrocarbon conversions were obtained at 900 °C, variation was noticed in the main product distribution on the different noble metal catalysts (table 5). Carbon monoxide was formed especially on Pt and ZrO_2, whereas the concentrations of H_2 and CO_2 were highest on the Pd- and Rh-containing catalysts. Doubtless, the water gas shift reaction (WGS, equation 5) was affecting the product distribution. Hence, the product distribution as such did not represent the catalyst selectivity for ATR reactions.

$$H_2O + CO \Leftrightarrow H_2 + CO_2 \qquad (5)$$

The molar ratio of ATR to the oxidation reaction can be calculated from the concentrations of the product gases (ATR/OX, equation 6). This ratio reveals the catalyst selectivity toward ATR, because the WGS equilibrium does not affect it.

$$\mathrm{ATR/OX} = \frac{[H_2] + [CO]}{[H_2O] + [CO_2]} \qquad (6)$$

Bimetallic $Rh_{0.21}Pt_{0.16}$ was the most selective catalyst for ATR of the *n*-dodecane–toluene mixture, though the calculated ATR/OX molar ratio was close to the thermodynamic equilibrium on all Rh-containing catalysts calcined at 700 °C. On Pd, the calculated ratio approached the thermodynamic equilibrium above 800 °C (figure 4), whereas on Pt catalysts and ZrO_2 it remained well below the thermodynamic equilibrium indicating lower selectivity for ATR reactions and more intensive oxidation. The selectivity of the Pt catalysts improved with temperature, however. For toluene, the thermodynamic equilibrium was only achieved on Rh.

3.2.3. Temperature profile measurements

The thermoneutrality of the ATR system was examined by comparing the catalyst bed temperatures during the ATR experiments. Figure 5 presents the temperature profiles of the catalyst bed (Rh, Pd, Pt, ZrO_2) measured

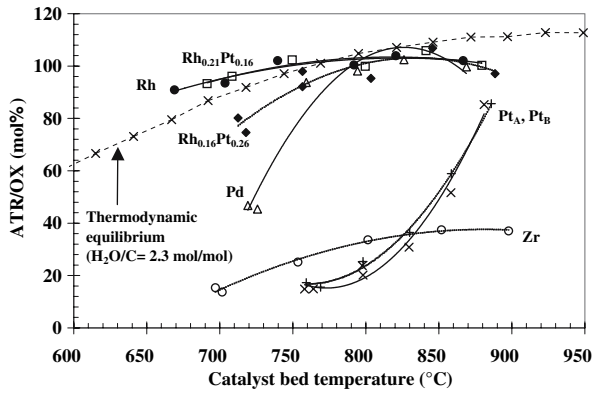

Fig. 4 ATR of the *n*-dodecane–toluene mixture, ATR/OX molar ratio on $Rh_{0.21}Pt_{0.16}$ (□), $Rh_{0.16}Pt_{0.26}$(◆), Rh (●), Pd (△), Pt_A (+), Pt_B (×), and ZrO_2 (○) catalysts. GHSV = 3.0×10^5 L/h, H_2O/C = 2.3 mol/mol. Abbreviations: A = nitrate, B = tetraamine nitrate precursor.

when the furnace temperature was set to 700 °C. The temperature profile varied with the temperature, the feedstock, the noble metal, and the GHSV.

On the Rh catalysts, ATR of *n*-dodecane was endothermic over the whole temperature range (700–900 °C). On the other monometallic catalysts the overall reaction of ATR became endothermic only at higher temperatures. These results confirm that the Rh catalyst was most active for endothermic SR reactions, whereas on Pt and Pd catalysts and on the support, exothermic oxidation reactions took place in front of the catalyst bed. The SR activity of the Pt and Pd catalysts increased with temperature, however. ATR of toluene was exothermic on all the studied catalysts, including Rh (figure 5). Probably due to the larger amount of O_2 fed to the reactor than was needed for thermoneutrality of ATR [9].

3.2.4. Catalyst deactivation

The deactivation of the catalysts was followed along the ATR cycle (6 h). At high temperatures, the deactivation did not markedly affect the conversions or product distribution. However, when a return was made to the initial reaction temperature (700 °C), a decrease in *n*-dodecane conversion was noticed on the Pd and Rh catalysts with both calcination temperatures. Deactivation of the Rh catalyst, but not of the other catalysts, was also noticed in ATR of toluene. On Rh, a plateau in the conversion curve of toluene appeared at 800 °C, and the conversion decreased from 98% at 700 °C to 86% at the end of the ATR cycle (figure 2b). Furthermore, an increase in the catalyst bed temperature and a pressure drop over the catalyst bed were noticed on the Rh catalysts.

The ATR cycle was followed by a regeneration step. The formation of carbon dioxide and water during the catalyst regeneration with air indicated coke accumulation. Although the evaluation was only

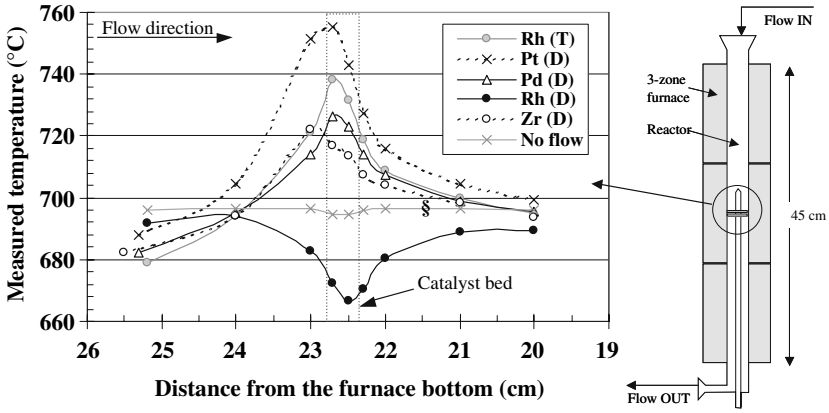

Fig. 5 Temperature profiles of the reactor in ATR of *n*-dodecane (D) or toluene (T) on Rh (●), Pd (△), Pt_A (×), and ZrO_2 (○) catalysts at temperature set to 700 °C. GHSV = 3.0×10^5 L/h, H_2O/C = 3 mol/mol.

Table 6
Loss in metal loading and coke accumulation on noble metal catalysts tested in ATR of the *n*-dodecane–toluene mixture

Catalyst	Loss in metal loading (mol%)	Coke accumulation (wt%)
$Rh_{0.16}Pt_{0.26}$	5.5 (Rh), 3.1 (Pt)	1.4
$Rh_{0.21}Pt_{0.16}$	–	0.8
Rh	30.8	0.9
Rh (900)*	n.a.	6.0
Pd	–	1.5
Pt_A	6.3	2.0
Pt_B	10.7	1.1

Abbreviations: A = nitrate, B = tetraamine nitrate precursor.
* The calcination temperature was 900 °C.

semi-quantitative, coke formation was clearly greatest on the Rh (900) catalyst calcined at 900 °C, and then on Pd and Pt catalysts (table 6). Moreover, almost twice as much coke was formed on the bimetallic catalyst with the higher Pt loading ($Rh_{0.16}Pt_{0.26}$, Rh/Pt = 1.2 mol/mol) as on the bimetallic catalyst with the lower loading ($Rh_{0.21}Pt_{0.16}$, Rh/Pt = 2.4 mol/mol). In addition, thermal cracking occurred on $Rh_{0.16}Pt_{0.26}$ at higher temperatures indicating a loss of activity. Even though coke formation is generally strongly related to thermal cracking and the formation of ethene [35], here coke accumulation did not correlate to the formation of ethene that was strongest on ZrO_2 and then on the Pt catalysts. Furthermore, substantially more coke was formed in reactions of *n*-dodecane than in reactions of toluene.

The metal loadings of the catalysts were measured after testing in ATR of the hydrocarbon mixture (table 1). During the ATR experiment, about 30 mol% of Rh and 10 mol% of Pt were lost from the monometallic catalysts (table 6). Probably, volatile Rh and Pt compounds were formed in the oxidative reforming conditions and these evaporated from the catalyst surface at high temperatures [36]. Considering the high reaction temperature (700–900 °C), the weak stability of the catalysts was probably a consequence of the low calcination temperature (700 °C). Nonetheless, bimetallic RhPt catalysts turned out to be thermally more stable than monometallic Rh and Pt catalysts. The coke formation on $Rh_{0.21}Pt_{0.16}$ catalyst with Rh/Pt ratio of 2.4 mol/mol was low (table 6), moreover, and no decrease in catalyst performance was observed during ATR.

4. Conclusions

Zirconia-supported Rh, Pd, and Pt catalysts were compared in ATR reactions of *n*-dodecane, toluene, and their mixture at 700–900 °C. In addition, bimetallic RhPt catalysts were studied in ATR of the hydrocarbon mixture. The H_2 and CO chemisorption uptakes were much higher on the Rh and Pd catalysts than on the Pt catalysts and the support. However, the stoichiometric ratio of the surface metal and the adsorbed CO could not be defined, as linear, bridged, and multibonded CO adsorption states were all present on the catalysts.

The Rh-containing catalysts were the most active toward ATR reactions; on the other noble metal catalysts (Pt and Pd) and on ZrO_2, exothermic oxidation reactions and thermal cracking of *n*-dodecane took place. The ATR activity of the Pd catalyst increased with temperature, however, almost to the level of the Rh catalysts. Still, the thermodynamic equilibrium of the ATR/OX ratio was reached only on Rh-containing catalysts, indicating that they were most selective catalysts toward ATR reactions. Indeed, the product distribution was highly dependent on the catalyst activity.

The thermal stability of the most active, Rh catalyst was weak, but it improved when Rh was combined with Pt in bimetallic RhPt catalysts. Thermal cracking reactions were still observed at Rh/Pt molar ratio of 1.2 ($Rh_{0.16}Pt_{0.26}$), and the more favorable Rh loading was 0.21 wt%, with Rh/Pt molar ratio of 2.4 ($Rh_{0.21}Pt_{0.16}$).

Acknowledgments

Hannu Revitzer is thanked for the metal loading determination and Arto Mäkinen is thanked for the chemisorption measurements. Financial support was received from VTT (Technical Research Center of Finland) and Tekes (The Finnish Funding Agency for Technology and Innovation).

References

[1] L.J. Pettersson and R. Westerholm, Int. J. Hydrogen Energy 26 (2001) 243.
[2] J.M. Ogden, M.M. Steinbugler and T.G. Kreutz, J. Power Sour. 79 (1999) 143.
[3] M. Krumpelt, T.R. Krause, J.D. Carter, J.P. Kopasz and S. Ahmed, Catal. Today 77 (2002) 3.
[4] J.R. Rostrup-Nielsen, in: *Catalysis Science and Technology*, J.R. Anderson and M. Boudart (eds. 5(Springer-Verlag, Berlin, 1984)ch 1.
[5] L.F. Brown, Int. J. Hydrogen Energy 26 (2001) 381.
[6] R.K. Kaila and O.A.I. Krause, Stud. Surf. Sci. Catal. 147 (2004) 247.
[7] D.L. Trimm and Z.I. Önsan, Cat. Rev. – Sci. Eng. 43(1&2) (2001) 31.
[8] D.A. Hickmann, E.A. Haupfear and L.D. Schmidt, Catal. Lett. 17 (1993) 223.
[9] R.K. Kaila and O.A.I. Krause, Int. J. Hydrogen Energy 31 (2006) 1934.
[10] C. Palm, R. Cremer, R. Peters and D. Stolten, J. Power Sour. 106 (2002) 231.
[11] J.B. Claridge, M.L.H. Green, S.C. Tsang, A.P.E. York, A.T. Ashcroft and P.D. Battle, Catal. Lett. 22 (1993) 299.
[12] T. Suzuki, H. Iwanami and T. Yoshinari, Int. J. Hydrogen Energy 25 (2000) 119.
[13] Anon., Kitco Inc., Historic Charts, Rhodium Monthly Averages 1972 – Present, http://www.kitco.com/charts/historicalrhodium.html, September 6, 2006.
[14] R.M. Ormerod, in: *High Temperature Solid Oxide Fuel Cells: Fundamentals, Design and Applications*., S.C. Singhal and K. Kendall (eds.(Elsevier, Cornwall, 2003)ch. 12.
[15] P. Fornasiero, J. Kašpar, V. Sergo and M. Graziani, J. Catal. 182 (1999) 56.
[16] V. Ragaini, R. Giannantonio, P. Magni, L. Lucarelli and G. Leofanti, J. Catal. 146(1) (1994) 116.
[17] Z.L. Zhang, A. Kladi and X.E. Verykios, J. Mol. Catal. 89 (1994) 229.
[18] M.M.V.M. Souza, D.A.G. Aranda and M. Schmal, J. Catal. 204 (2001) 498.
[19] X. Wang, R.J. Gorte and J.P. Wagner, J. Catal. 212 (2002) 225.
[20] A. Guerreri-Ruiz, S. Yang, Q. Xin, A. Maroto-Valiente, M. Benito-Gonzalez and I. Rodriguez-Ramos, Langmuir 16 (2000) 8100.
[21] S.M.K. Airaksinen, M. Bañares and A.O.I. Krause, J. Catal. 230 (2005) 516.
[22] A. Roine, HSC Chemistry for Windows 5.11. Outokumpu Research, 2003.
[23] J.D. Tate and P. Jaakkola, J. Process Anal. Chem. 5(1,2) (2000) 15.
[24] A. Hakuli, A. Kytökivi, E.-L. Lakomaa and A.O.I. Krause, Anal. Chem. 67 (1995) 1881.
[25] C. Mazzocchia, P. Gronchi, E. Tempesti, E. Guglielminotti and L. Zanderighi, J. Mol. Catal. 60 (1990) 283.
[26] O. Dulaurent, K. Chandes, C. Bouly and D. Bianchi, J. Catal. 188 (1999) 237.
[27] E.V. Benvenutti, L. Franken and C.C. Moro, Langmuir 15 (1999) 8140.
[28] O. Dulaurent and D. Bianchi, Appl. Catal. A207 (2001) 211.
[29] V. Perrichon, L. Retailleau, P. Bazin, M. Daturi and J.C. Lavalley, Appl. Catal. A260 (2004) 1.
[30] J. Wei and E. Iglesia, J. Catal. 225 (2004) 116.
[31] K. Polychronopoulou, J.L.G. Fierro and A.M. Efstathiou, J. Catal. 228 (2004) 417.
[32] S.Y. Choung, M. Ferrandon and T. Krause, Catal. Today 99 (2005) 257.
[33] S. Trautmann and M. Baerns, J. Catal. 150 (1994) 335.
[34] E. Guglielminotti, F. Pinna, M. Rigoni, G. Strukul and L. Zanderighi, J. Mol. Catal. 103(2) (1995) 105.
[35] F. Joensen and J.R. Rostrup-Nielsen, J. Power Sour. 105 (2002) 195.
[36] J. Zhu, Catalytic Partial Oxidation of Methane to Synthesis Gas over ZrO_2-based Defective Oxides, Doctoral Thesis (Printpartners Ipskamp B. V., Enschede, 2005) 118 p.